Article

Synthesis, Electronic Structure, and Electron Transfer Dynamics of (Aryl)ethynyl-Bridged Donor–Acceptor Systems

Naomi P. Redmore, Igor V. Rubtsov, and Michael J. Therien

J. Am. Chem. Soc., **2003**, 125 (29), 8769-8778• DOI: 10.1021/ja021278p • Publication Date (Web): 27 June 2003

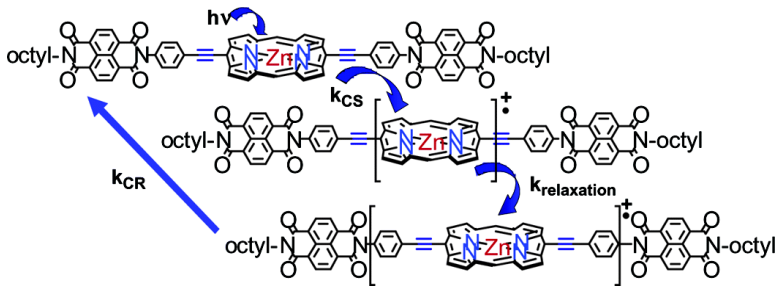

More About This Article

Additional resources and features associated with this article are available within the HTML version:

- Supporting Information
- Links to the 8 articles that cite this article, as of the time of this article download
- Access to high resolution figures
- Links to articles and content related to this article
- Copyright permission to reproduce figures and/or text from this article

View the Full Text HTML

J|A|C|S
ARTICLES
Published on Web 06/27/2003

Synthesis, Electronic Structure, and Electron Transfer Dynamics of (Aryl)ethynyl-Bridged Donor−Acceptor Systems

Naomi P. Redmore, Igor V. Rubtsov, and Michael J. Therien*

Contribution from the Department of Chemistry, University of Pennsylvania, Philadelphia, Pennsylvania 19104-6323

Received October 17, 2002; Revised Manuscript Received January 30, 2003; E-mail: therien@a.chem.upenn.edu

Abstract: The ET dynamics of a series of donor−spacer−acceptor (D−Sp−A) systems featuring (porphinato)zinc(II), (aryl)ethynyl bridge, and arene diimide units were investigated by pump−probe transient absorption spectroscopy. Analysis of these data within the context of the Marcus−Levich−Jortner equation suggests that the π-conjugated (aryl)ethynyl bridge plays an active role in the charge recombination (CR) reactions of these species by augmenting the extent of (porphinato)zinc(II) cation radical electronic delocalization; this increase in cation radical size decreases the reorganization energy associated with the CR reaction and thereby attenuates the extent to which the magnitudes of the CR rate constants are solvent dependent. The symmetries of porphyrin-localized HOMO and HOMO-1, the energy gap between these two orbitals, and D−A distance appear to play key roles in determining whether the (aryl)-ethynyl bridge simply mediates electronic superexchange or functions as an integral component of the D and A units.

Introduction

Electron transfer (ET) reactions play fundamental roles in solar energy conversion. Mechanistic studies of photoinduced charge separation (CS) and thermal charge recombination (CR) reactions in covalently linked donor−acceptor (D−A) arrays have probed how varying magnitudes of thermodynamic driving force ($\Delta G°$), reorganization energy (λ), and electronic coupling (H_{AB}) control such ET processes.[1,2] While there exist some notable exceptions,[3−7] the vast majority of such investigations involving porphyrin-containing donor−spacer−acceptor (D−Sp−A) compounds have focused on systems in which the D, Sp, and A units remain electronically distinct within the excited and charge-transfer states pertinent to the CS and CR reactions. Hence, while the D, Sp, and A units of these assemblies generally feature extensive π-conjugation, design criteria have typically ensured weak electronic coupling between these conjugated components;[1,2] as a result, relatively little is known regarding the photophysics and ET dynamics of D−Sp−A assemblies in which strong electronic coupling mixes D, Sp, and A electronic states effectively.

This contribution details the potentiometric properties, photophysics, and the photoinduced CS and thermal CR dynamics for a series of ET assemblies comprising a (porphinato)zinc(II) donor, an (aryl)ethynyl bridge (Sp), and either a pyromellitimide (PI) or naphthylic diimide (NI) acceptor unit (Figure 1). These D−Sp−A arrays feature D-to-Sp connectivity in which a *meso*-porphyryl-ethyne substituent directly links the conjugated macrocycle to the aromatic spacer units.[8] We show that this combination of D, Sp, and A moieties gives rise to atypical dynamics following the CS events in these systems; these dynamics derive from the π-conjugated nature of the intervening (aryl)ethynyl bridge and the electronic structure of the high-lying filled orbitals of the porphyryl and diimide units.

(1) (a) Wasielewski, M. R.; Niemczyk, M. P.; Svec, W. A.; Pewitt, E. B. *J. Am. Chem. Soc.* **1985**, *107*, 1080−1082. (b) Irvine, M. P.; Harrison, R. J.; Beddard, G. S. *Chem. Phys.* **1986**, *104*, 315−324. (c) Joran, A. D.; Leland, B. A.; Felker, P. M.; Zewail, A. H.; Hopfield, J. J.; Dervan, P. B. *Nature* **1987**, *327*, 508−511. (d) Closs, G. L.; Miller, J. R. *Science* **1988**, *24*, 440−446. (e) Finckh, P.; Heitele, H.; Michel-Beyerle, M. E. *Chem. Phys.* **1989**, *138*, 1−10. (f) Beratan, D. N.; Onuchic, J. N. *Adv. Chem. Ser.* **1991**, 71−90. (g) Gust, D.; Moore, T. A. *Photosynth. Model Sys.* **1991**, *159*, 103−151. (h) Helms, A.; Heiler, D.; McLendon, G. *J. Am. Chem. Soc.* **1991**, *113*, 4325−4327. (i) Rodriguez, J.; Kirmaier, C.; Johnson, M. R.; Friesner, R. A.; Holten, D.; Sessler, J. L. *J. Am. Chem. Soc.* **1991**, *113*, 1652−1659. (j) Jordan, K. D.; Paddon-Row, M. N. *Chem. Rev.* **1992**, *92*, 395−410. (k) Liu, J.-Y.; Bolton, J. R. *J. Phys. Chem.* **1992**, *96*, 1718−1725. (l) Chambron, J.-C.; Chardon-Noblat, S.; Harriman, A.; Heitz, V.; Sauvage, J.-P. *Pure Appl. Chem.* **1993**, *65*, 2343−2349. (m) Heitele, H. *Angew. Chem., Int. Ed. Engl.* **1993**, *32*, 359−377. (n) Osuka, A.; Nakajima, S.; Maruyama, K.; Magata, N.; Asahi, T.; Yamazaki, I.; Nishimura, Y.; Ohno, T.; Nozaki, K. *J. Am. Chem. Soc.* **1993**, *115*, 4577−4589. (o) Farid, R. S.; Chang, I.-J.; Winkler, J. R.; Gray, H. B. *J. Phys. Chem.* **1994**, *98*, 5176−5179. (p) Barbara, P. F.; Meyer, T. J.; Ratner, M. A. *J. Phys. Chem.* **1996**, *100*, 13148−13168. (q) Häberle, T.; Hirsch, J.; Pöllinger, F.; Heitele, H.; Michel-Beyerle, M. E.; Anders, C.; Döhling, A.; Krieger, C.; Rückemann, A.; Staab, H. A. *J. Phys. Chem.* **1996**, *100*, 18269−18274. (r) Paulson, B. P.; Curtiss, L. A.; Bal, B.; Closs, G. L.; Miller, J. R. *J. Am. Chem. Soc.* **1996**, *118*, 378−387. (s) Kuciauskas, D.; Liddell, P. A.; Hung, S.-C.; Lin, S.; Stone, S.; Seely, G. R.; Moore, A. L.; Moore, T. A.; Gust, D. *J. Phys. Chem. B* **1997**, *101*, 429−440. (t) Roest, M. R.; Oliver, A. M.; Paddon-Row, M. N.; Verhoeven, J. W. *J. Phys. Chem. A* **1997**, *101*, 4867−4871. (u) Sakata, Y.; Imahori, H.; Tsue, H.; Higashida, S.; Akiyama, T.; Yoshizawa, E.; Aoki, M.; Yamada, K.; Hagiwara, K.; Taniguchi, S.; Okada, T. *Pure Appl. Chem.* **1997**, *69*, 1951−1956. (v) Macatangay, A. V.; Endicott, J. F.; Song, X. *J. Phys. Chem. A* **1998**, *102*, 7537−7540. (w) Jones, G., II; Lu, L. N.; Fu, H. N.; Farahat, C. W.; Oh, C.; Greenfield, S. R.; Gosztola, D. J.; Wasielewski, M. R. *J. Phys. Chem. B* **1999**, *103*, 572−581. (x) Klumpp, T.; Linsenmann, M.; Larson, S. L.; Limoges, B. R.; Bürssner, D.; Krissinel, E. B.; Elliott, C. M.; Steiner, U. E. *J. Am. Chem. Soc.* **1999**, *121*, 1076−1087. (y) Page, C. C.; Moser, C. C.; Chen, X.; Dutton, P. L. *Nature* **1999**, *402*, 47−52. (z) Winkler, J. R.; Di Billo, A. J.; Farrow, N. A.; Richards, J. H.; Gray, H. B. *Pure Appl. Chem.* **1999**, *71*, 1753−1764.

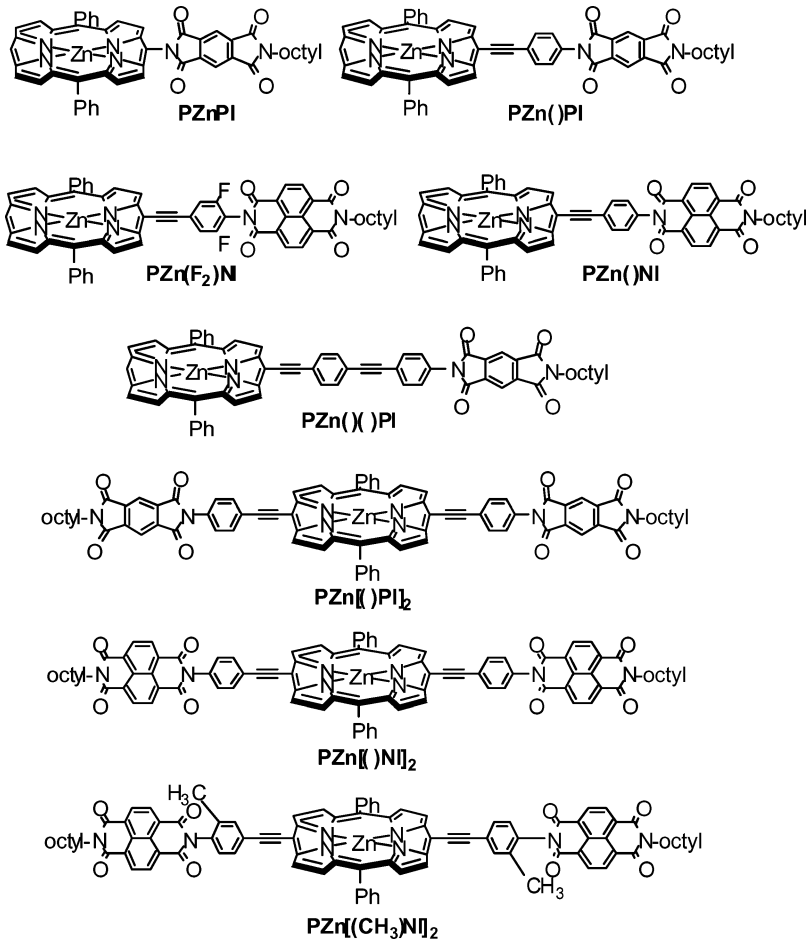

Figure 1. Rigid D−Sp−A systems featuring (aryl)ethynyl bridging units.

Experimental Section

Materials. All manipulations were carried out as previously reported;[9] synthetic details are described in the Supporting Information and in an earlier contribution.[9]

Instrumentation. Electronic spectra were recorded on an OLIS UV/vis/NIR spectrophotometry system that is based on the optics of a Cary 14 spectrophotometer. NMR spectra were recorded on either 250 MHz AC-250, or 360 MHz Brüker spectrometers. Cyclic voltammetric responses were recorded on an EG&G Princeton Applied Research model 273A potentiostat/galvanostat.

Pump−Probe Transient Absorption Spectroscopic Measurements. Transient absorption spectra were obtained using standard pump−probe methods. Optical pulses, centered at 775 nm, were generated using a Ti:sapphire laser (Clark-MXR, CPA-2001). Optical parametric amplifiers (near-IR and visible OPAs, Clark-MXR) generate excitation pulses tunable in wavelength from the UV through the near-IR region; a white light continuum served as the probe beam. After passing through the sample, the probe light was focused onto the entrance slit of the computer-controlled image spectrometer (SpectraPro-150, Acton Research Corp.). The baseline noise level in these transient absorption experiments corresponded to ∼0.2 mOD/s of signal accumulation. The time resolution is probe-wavelength-dependent; in these experiments the fwhm of the instrument response function varied between 140 and 200 fs. A detailed description of the transient optical apparatus has recently been reported.[10] All experiments were carried out at room temperature (23 ± 1 °C).

Electronic Structure Calculations. Frontier orbital energies for the [5,15-bis[(4′-substituted-aryl)ethynyl]-10,20-diphenylporphinato]zinc(II) compounds were determined using CAChe ZINDO with standard INDO-1 semiempirical parameters at a configuration interaction (CI) level = 20.[11] For all the model complexes, the central zinc metal atoms were assigned a dsp^2

(2) (a) Miller, S. E.; Lukas, A. S.; Marsh, E.; Bushard, P.; Wasielewski, M. R. *J. Am. Chem. Soc*. **2000**, *122*, 7802−7810. (b) Napper, A. M.; Read, I.; Waldeck, D. H. *J. Am. Chem. Soc*. **2000**, *122*, 5220−5221. (c) Sykora, M.; Maxwell, K. A.; DeSimone, J. M.; Meyer, T. J. *Proc. Natl. Acad. Sci. U.S.A.* **2000**, *97*, 7687−7691. (d) Tsue, H.; Imahori, H.; Kaneda, T.; Tanaka, Y.; Okada, T.; Tamaki, K.; Sakata, Y. *J. Am. Chem. Soc*. **2000**, *122*, 2279−2288. (e) Imahori, H.; Guldi, D. M.; Tamaki, K.; Yoshida, Y.; Luo, C.; Sakata, Y.; Fukuzumi, S. *J. Am. Chem. Soc.* **2001**, *123*, 6617−6628. (f) Kilså, K.; Kajanus, J.; Macpherson, A. N.; Mårtensson, J.; Albinsson, B. *J. Am. Chem. Soc*. **2001**, *123*, 3069−3080. (g) Sikes, H. D.; Smalley, J. F.; Dudek, S. P.; Cook, A. R.; Newton, M. D.; Chidsey, C. E. D.; Feldberg, S. W. *Science* **2001**, *291*, 1519−1523.
(3) Foley, M. J.; Singer, L. A. *J. Phys. Chem.* **1994**, *98*, 6430−6435.
(4) Biswas, M.; Nguyen, P.; Marder, T. B.; Khundkar, L. R. *J. Phys. Chem. A* **1997**, *101*, 1689−1695.
(5) Davis, W. B.; Svec, W. A.; Ratner, M. A.; Wasielewski, M. R. *Nature* **1998**, *396*, 60−63.
(6) Nakano, A.; Osuka, A.; Yamazaki, T.; Nishimura, Y.; Akimoto, S.; Yamazaki, I.; Itaya, A.; Murakami, M.; Miyasaka, H. *Chem.−Eur. J.* **2001**, *7*, 3134−51.
(7) Pourtois, G.; Belijonne, D.; Cornil, J.; Ratner, M. A.; Brédas, J. L. *J. Am. Chem. Soc.* **2002**, *124*, 4436−4447.
(8) LeCours, S. M.; DiMagno, S. G.; Therien, M. J. *J. Am. Chem. Soc*. **1996**, *118*, 11854−11864.
(9) Redmore, N. P.; Rubtsov, I. V.; Therien, M. J. *Inorg. Chem.* **2002**, *41*, 566−570.
(10) Rubtsov, I. V.; Susumu, K.; Rubstov, G. I.; Therien, M. J. *J. Am. Chem. Soc*. **2003**, *125*, 2687−2696.
(11) ZINDO software was provided by CAChe Scientific, Beaverton, OR.

(square planar) geometry, and the 10- and 20-*meso* phenyl groups were fixed at 90° with respect to the porphyrin plane. Geometry optimizations were carried out using the MOPAC-AM1 method. The convergence criteria for these restricted Hartree−Fock (RHF) self-consistent field (SCF) calculations required the root-mean-squared (rms) difference in the elements of the density matrix to be below 10^{-6} on two successive SCF cycles.

General Procedure for the Preparation of *N*-(4′-Halophenyl)-*N*′-(octyl)diimide Complexes. The precursors, *N*-octylbenzene-1,2-dicarboxyanhydride-4,5-dicarboximide (**1**) and *N*-octylnaphthalene-1,8-dicarboxyanhydride-4,5-dicarboximide (**2**), were prepared by cyclization of 1,2,4,5-pyromellitic dianhydride or 1,8,4,5-naphthylic dianhydride with *n*-octylamine in refluxing DMF solution.[12] Either **1** or **2** (∼200 mg, 530 μmol) was added under N_2 to a 50-mL round-bottomed flask which was equipped with a reflux condenser. DMF (10 mL) was added to the flask, and the mixture was heated to 80 °C and stirred rapidly to form a fine suspension. CaO (5 mg) and a 4-haloaniline (∼125 mg, 580 μmol) were then added to the mixture. After refluxing for 12 h, the hot reaction mixture was filtered, and the collected solid was washed with hot hexanes. The residual solid was collected as product. Complete details of the synthesis and characterization of [5-[4′-(*N*-(*N*′-octyl)pyromellitic diimide)-phenyl)ethynyl]-10,20-diphenylporphinato]zinc(II) (**PZn( )PI**), [5-[4′′-(*N*-(*N*′-octyl)naphthylic diimide)phenyl)ethynyl]-10,20-diphenylporphinato]zinc(II) (**PZn( )NI**), [5-[2′,5′-difluoro-4′-(*N*-(*N*′-octyl)naphthylic diimide)phenyl)ethynyl]-10,20-diphenylporphinato]zinc(II) (**PZn(F_2)NI**), [5,15-bis[4′-(*N*-(*N*′-octyl)-pyromellitic diimide)phenyl)ethynyl]-10,20-diphenylporphinato]-zinc(II), and [5-[4′-[4′′-(*N*′(*N*′′-octyl)pyromellitic diimide)-phenyl)ethynyl]phenyl)ethynyl]-10,20-diphenylporphinato]-zinc(II) (**PZn( )( )PI**) can be found in the Supporting Information.

General Procedure for the Preparation of) [5-[4′-(*N*-(*N*′-octyl)pyromellitic/naphthylic diimide)aryl)ethynyl]-10,20-diphenylporphinato]zinc(II) Complexes. [5-Ethynyl-10,20-diphenylporphinato]zinc(II) (55 mg, 100 μmol),[13,14] the desired *N*-(4′-halophenyl)-*N*′-(octyl)diimide species (∼50 mg, 90 μmol), CuI (2 mg, 12 μmol), $Pd(Ph_3)_2Cl_2$ (4 mg, 5 μmol) were combined in a 25-mL Schlenk tube under N_2. An anhydrous, degassed 10-mL mixture of 1:1:1 diisopropylamine:THF: acetonitrile was added to the Schlenk tube via cannula transfer. The reaction mixture was stirred at 40 °C for 12−24 h, until TLC (7:3 hexanes:THF) indicated that the starting material had been consumed. The solution was cooled to room temperature, diluted with chloroform (100 mL), washed with saturated aqueous ammonium chloride (50 mL), distilled water (50 mL), and saturated aqueous sodium chloride (50 mL), and dried over magnesium sulfate. After filtration to remove drying agent, the filtrate was passed through a plug of silica gel ($CHCl_3$), concentrated, and purified by size exclusion chromatography (THF). The first green fraction eluted from the column was concentrated under vacuum to yield the desired [5-(4′-(*N*-(*N*′-octyl)pyromellitic/naphthylic diimide)aryl)ethynyl]-10,20-diphenylporphinato]zinc(II) complex. Samples suitable for transient optical studies were prepared by subsequent silica gel chromatography (CH_2Cl_2) and filtration through a 3-μm glass filter to remove suspended particulates. Complete details of the synthesis and characterization of [5,15-bis[4′-(*N*-(*N*′-octyl)pyromellitic diimide)phenyl)ethynyl]-10,20-diphenyl-porphinato]zinc(II) (**PZn[( )PI]$_2$**), [5,15-bis[4′-(*N*-(*N*′-octyl)-naphthylic diimide)phenyl]ethynyl]-10,20-diphenylporphinato]-zinc(II) (**PZn[( )NI]$_2$**), and [5,15-bis[3′-methyl-4′-(*N*-(*N*′-octyl)-naphthylic diimide)phenyl)ethynyl]-10,20-diphenylporphinato]-zinc(II) (**PZn[(CH_3)NI]$_2$**) can be found in the Supporting Information.

Results and Discussion

Synthesis. The synthesis of **PZn[( )NI]$_2$** is illustrative of the synthesis of these (phenyl)ethynyl-bridged D−A systems. Naphthylic dianhydride was converted to the corresponding imide-anhydride precursor **2** (*N*-(*N*′-octyl)-naphthalene-1,8-dicarboxyanhydride-4,5-dicarboximide), using methodology described by Wasielewski.[12] *N*-(4-iodophenyl)-*N*′-octyl diimide can serve as a substrate in a palladium-catalyzed cross-coupling reaction with either [5-ethynyl-10,20-diphenylporphinato]zinc(II) or [5,15-diethynyl-10,20-diphenylporphinato]zinc(II)[13,14] to yield the desired D−Sp−A species (Scheme S1, Supporting Information). [5-[4′-[4′′-(*N*′-(*N*′′-Octyl)pyromellitic diimide)phenyl)-ethynyl]phenyl)ethynyl]-10,20-diphenylporphinato]zinc(II) (**PZn-( )( )PI**) (Figure 1), which features an extended conjugated bridge, was prepared by the one-pot palladium-catalyzed cross-coupling reaction between *N*-(4′-iodophenyl)-*N*-(*n*-octyl)pyromellitic diimide, 1,4-diethynylbenzene, and 5-bromo-(10,20-diphenylporphinato)zinc(II) (Scheme S2, Supporting Information).

Transient Absorption Spectra. PZnPI. The ET dynamics for **PZn−PI** have been reported previously.[9] Photoexcitation of **PZn−PI** in dichloromethane results in the formation of a porphyrin-based singlet excited state **^{1}(PZn)*-PI** which undergoes a CS reaction with a time constant (τ_{CS}) of 770 fs, followed by a CR reaction with τ_{CR} = 5.2 ps. The signature transient absorption for both the PI anion radical (sharp absorption at ∼710 nm) and the PZn cation radical (broad absorptions at ∼470 and 700 nm) can be identified clearly in the pump−probe spectroscopic experiments. These spectra serve as a benchmark for comparison to those manifest by the D−Sp−A systems in which a conjugated bridging unit links the PZn and PI/NI moieties.

PZn( )PI. The ET dynamics that follow electronic excitation of **PZn( )PI**, in which a (4′-phenyl)ethynyl bridge separates D from A, differ markedly from that exhibited by **PZn−PI**. The transient optical spectra obtained in CH_2Cl_2 show evidence for vibrational relaxation and hot ground-state formation in addition to dynamics associated with the CS and CR reactions (Figure 2). Photoinduced CS and thermal CR rate constants were determined from a multiwavelength global fit of the visible domain transients. (Representative wavelength ranges that are particularly useful in this regard include ∼470−530 and ∼680−740 nm, where the radical anions of NI and PI, respectively, have strong absorbances, and wavelengths near 500 nm, which can be utilized to track the relative populations of the excited PZn singlet state and its corresponding porphyrin cation radical, $(PZn)^{\bullet+}$.)

The **PZn( )PI** transient absorption spectra observed immediately following electronic excitation (e.g., 260 fs time delay, Figure 2) are dominated by absorptive and emissive contribu-

(12) Greenfield, S. R.; Svec, W. A.; Gosztola, D.; Wasielewski, M. R. *J. Am. Chem. Soc.* **1996**, *118*, 6767−6777.
(13) Lin, V. S.-Y.; DiMagno, S. G.; Therien, M. J. *Science* **1994**, *264*, 1105−1111.
(14) Lin, V. S.-Y.; Therien, M. J. *Chem.−Eur. J.* **1995**, *1*, 645−651.

Table 1. Charge Separation and Charge Recombination Dynamical Data Determined from Pump−Probe Transient Absorption Spectroscopic Experiments

compound	solvent	τ_{CS} (ps)	k_{CS} (s^{-1})	τ_{CR} (ps)	k_{CR} (s^{-1})	τ_{CR}/τ_{CS}
PZnPI	CH_2Cl_2	0.77	1.3×10^{12}	5.2	1.9×10^{11}	6.8
PZn( )PI	CH_2Cl_2	24.4	4.1×10^{10}	1.05	9.5×10^{11}	0.043
PZn( )( )PI	CH_2Cl2	65	1.5×10^{10}	564	1.8×10^{9}	8.7
PZn[( )PI]$_2$	$CH2Cl_2$	64	1.6×10^{10}	7	1.4×10^{11}	0.11
PZn( )NI	CH_2Cl_2	29	3.5×10^{10}	5.7	1.8×10^{11}	0.20
PZn(F_2)NI	CH_2Cl_2	29	3.5×10^{10}	4.4	2.3×10^{11}	0.15
PZn[( )NI]$_2$	CH_3CN	33	3.0×10^{10}	2.2	4.5×10^{11}	0.053
	CH_2Cl_2	23	4.3×10^{10}	6	1.6×10^{11}	0.6
	benzene	12	8.3×10^{10}	430	2.3×10^{9}	36
PZn[(CH_3)NI]$_2$	CH_3CN	45	2.2×10^{10}	4.8	2.1×10^{11}	0.07
	CH_2Cl_2	∼10	$\sim 1.0 \times 10^{11}$	∼10	$\sim 1.0 \times 10^{11}$	0.59
	benzene	15.5	6.5×10^{10}	74	1.4×10^{10}	4.8
	polystyrene	3.6	2.8×10^{11}	900	1.1×10^{9}	250

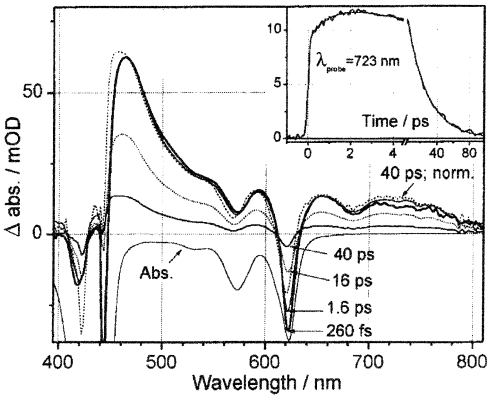

Figure 2. Transient absorption spectra of **PZn( )PI** in methylene chloride, with labeled time delays. Inset shows transient kinetics measured at 723 nm. Experimental conditions: $\lambda_{ex} = 630$ nm, temperature $= 23 \pm 1$ °C.

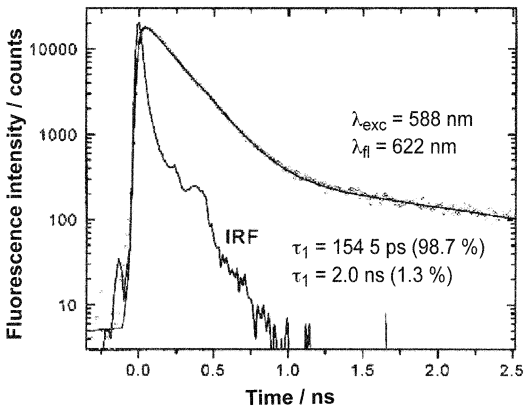

Figure 3. Fluorescence decay profile of **PZn( )PI** in acetonitrile solvent acquired by the time-correlated single-photon counting method. Experimental conditions: $\lambda_{ex} = 588$ nm, $\lambda_{fl} = 622$ nm.

tions associated with the porphyrin S_1-excited state, along with the expected ground-state bleach signatures; these spectra are analogous to those obtained for model compounds which lack an acceptor unit. Interestingly, (**PZn( )PI)*** exhibits stimulated emission (∼680 nm) coincident with that observed in the steady-state fluorescence spectrum; note that Figure 2 displays no appreciable transient absorptions that can be assigned to either the porphyrin cation radical or to the pyromellitimide anion radical species and that decay of the excited state spectrum occurs concomitantly with the recovery of the ground-state bleach component of the absorbance spectrum.

Characteristic times of 1.05 and 24.4 ps were obtained from a biexponential fit of the **PZn( )PI** transient data at 480 and ∼725 nm; as the charge-separated state does not dominate the spectrum, the 24.4 and 1.05 ps time constants were assigned to the CS and CR reactions, respectively (Table 1). These assignments were verified by fluorescence lifetime measurements determined by time-correlated single-photon counting spectroscopy (Figure 3) carried out in acetonitrile solvent. The τ_{CS} value determined by this method (154 ± 5 ps) is in good agreement with the CS time constant measured in CH_3CN solvent by pump−probe transient absorption spectroscopy ($\tau_{CS} = 150$ ps, see Supporting Information).

Transient Absorption Spectra of PZn( )NI, PZn(F_2)NI, PZn( )NI, and PZn( )PI$_2$. The general features of the pump−probe transient absorption spectra obtained for **PZn( )NI**, **PZn(F_2)NI, PZn[( )PI]$_2$**, and **PZn[( )NI]$_2$** (Figure 1, see Supporting Information) resemble those elucidated for **PZn( )PI** (Figure 2); the time constants calculated for the CS and CR reactions of these species are listed in Table 1. The spectra obtained over time domains ranging from approximately 100 fs to ∼10 ps consist largely of transient signals associated with the S_1 state, which is consistent with the observation of stimulated emission over this time domain. Rapid quenching of the S_1-excited state in these systems causes the difference spectra to decay quickly; similar behavior is seen for **PZn( )PI** (Figure 2).

For nonadiabatic ET reactions, as solvent polarity decreases, the dipolar state becomes less stabilized, decreasing and increasing $\Delta G°$ for the CS and CR reactions ($\Delta G°_{CS}$ and $\Delta G°_{CR}$), respectively (tabulated thermodynamic and metrical data for these compounds can be found in Table 2). At the same time, the diminished solvation of the charge-separated state in a less polar solvent decreases the total reorganization energy (λ_T) for CS reactions. This decrease in λ_T parallels a diminution in thermodynamic driving force in less polar solvents, causing ($\Delta G + \lambda_T$) and thus k_{CS} to exhibit weak solvent dependences.[15−18] For CR reactions in the Marcus inverted region, decreasing solvent polarity increases the energy of the charge-separated state; the concomitant decrease in the solvent reorganization energy (λ_S) makes the quantity ($\Delta G + \lambda_T$) more negative,

(15) Bixon, M.; Jortner, J. In *Electron Transfer-From Isolated Molecules to Biomolecules*; Prigogine, I., Rice, S. A., Eds.; John Wiley & Sons: New York, 1999; Vol. 106, pp 35−202.
(16) Bolton, J. R.; Archer, M. D. *Basic Electron-Transfer Theory*; 1991; pp 7−33.
(17) Chen, P.; Mecklenburg, S. L.; Meyer, T. J. *J. Phys. Chem.* **1993**, *97*, 13126−13131.
(18) Barbara, P. F.; Meyer, T. J.; Ratner, M. A. *J. Phys. Chem.* **1996**, *100*, 13148−13168.

Table 2. Thermodynamic and Metrical Data

compound	$E_{1/2}^{ox}$ [a] mV	$E_{1/2}^{red}$ mV	R_{DA} Å	$-\Delta G^0_{CS}$ [b,c] eV	$-\Delta G^0_{CR}$ eV	solvent
PZnPI	880	−860	8.3	0.55	1.55	CH_2Cl_2
PZn( )PI	650	−890	15	0.67	1.43	CH_2Cl_2
PZn( )( )PI	820	−810	21.7	0.54	1.56	CH_2Cl_2
PZn[( )PI]$_2$	850	−790	15	0.57	1.53	CH_2Cl_2
	855	−785		0.50	1.60	Bz[d]
PZn( )NI	780	−560	15.2	0.86	1.24	CH_2Cl_2
	780	−560		0.80	1.30	Bz
PZn(F$_2$)NI	860	−510	15.3	0.83	1.27	CH_2Cl_2
	880	−510		0.75	1.35	Bz
PZn[( )NI]$_2$	820	−570	15.2	0.81	1.29	CH_2Cl_2
		−570		0.75[e]	1.43[e]	Bz
PZn[(CH$_3$)NI]$_2$	810	−545	15.2	0.85	1.25	CH_2Cl_2
		−550		0.78[e]	1.40[e]	Bz

[a] Experimental conditions: [porphyrin] = 1.0 mM; [$TBAClO_4$] = 0.1 M; reference electrode = SCE; working electrode = glassy carbon; auxiliary electrode = Pt wire. $E_{1/2}^{ox}$ and $E_{1/2}^{red}$ values correspond respectively to the $PZn^{0/+}$ and $PI/NI^{-/0}$ potentials. These data are reported relative to SCE; the ferrocene/ferrocenium redox couple (0.43 V vs SCE) was used as the internal standard. [b] These values have been corrected for the Coulombic work term, $\Delta G(\epsilon)$. The D−A center-to-center distances were estimated from their MOPAC-determined minimum energy geometries. [c] The porphyrin lowest excited singlet state energy, $E(0,0)$, was determined from the overlap of the absorbance and emission spectra. [d] Bz = benzonitrile. [e] Assuming no significant change in the (D/D^+) potential from that determined in methylene chloride.

typically effecting a decrease the magnitude of the CR rate constant (k_{CR}). The CR reactions of covalently linked D−A dyads have, almost without exception,[19] been found to have negative ($\Delta G + \lambda$) values, indicating that these reactions lie within the Marcus inverted region. Consistent with this, (i) the magnitudes of k_{CR} reported for these D−Sp−A compounds are larger in more polar solvents, and (ii) the transient absorption spectra acquired for these species in highly nonpolar solvents such as benzene display stronger absorption signals from the CS state (Table 1).

Steady-State Electronic Absorption Spectra. PZn( )PI, **PZn( )NI**, **PZn(F$_2$)NI**, **PZn[( )PI]$_2$**, **PZn( )PI PZn[( )NI]$_2$**, **PZn[(CH$_3$)NI]$_2$**, and **PZn( )( )PI** display broadened and red-shifted Soret and Q-transitions in all solvents relative to the directly linked D−A compound **PZn−PI**, (see Supporting Information). Appending a cylindrically π-symmetric ethyne to the macrocycle *meso*-carbon position effects a significant splitting of the normally degenerate porphyrin *x*- and *y*-polarized excited states. This perturbation from the electronic spectra of conventional PZn complexes has been discussed previously.[8,20−24] For example, 5,15-diethynyl-10,20-diarylporphyrin manifests a broadened Soret transition as the *x*- and *y*-polarized B-state transitions are no longer isoenergetic; simplex fitting of the B-band shows that the splitting of the B_x and B_y states is on the order of ∼300 cm^{-1}.[24] *meso*-(Aryl)ethynyl substituents have been observed to effect larger splittings of the *x*- and *y*-polarized B states relative to an ethyne group,[8,13,20−23] with the energy gap between the $B_x(0,0)$ and $B_y(0,0)$ levels >2000 cm^{-1} when

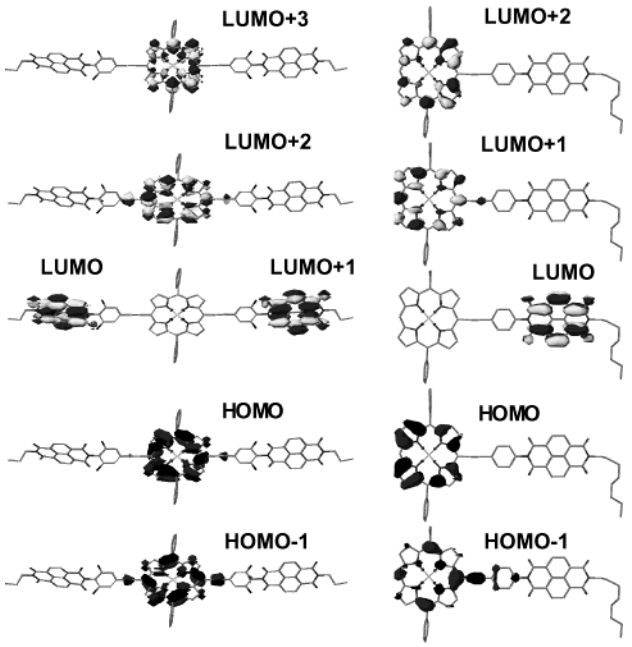

Figure 4. Frontier molecular orbitals of (A) **PZn[(F$_2$)NI]$_2$** and (B) **PZn( )NI**.

the PZn 5- and 15-(aryl)ethynyl substituents are electronically asymmetric.[23] Large magnitude splittings of the Q_x and Q_y transitions are also evident in such systems, with the $Q_x(0,0)$ state lying several hundred wavenumbers lower in energy with respect to its $Q_y(0,0)$ counterpart.[8,23] Interestingly, simplex spectral fitting analyses (data not shown) demonstrate that the magnitudes of the energetic splittings between the Q_x and Q_y transitions for these [5-[4′-(*N*-(*N*′-octyl)pyromellitic/naphthylic diimide)aryl)ethynyl]-10,20-diphenylporphinato]zinc(II) and [5,15-bis[4′-(*N*-(*N*′-octyl)pyromellitic/naphthylic diimide)aryl)-ethynyl]-10,20-diphenylporphinato]zinc(II) complexes are diminished with respect to the previously investigated 5,15-bis-[(4′-substituted-aryl)ethynyl]-10,20-diphenylporphinato]zinc(II) benchmarks[8,20−23] and are on the order of a few hundred wavenumbers (vide infra).

Electronic Structure Calculations. The frontier orbital (FO) energies for **PZn( )NI** and **PZn[(F$_2$)NI]$_2$** were determined using the ZINDO method at a CI level of 20 (Experimental Section); FOs for these species are displayed in Figure 4. Interestingly, in contrast to [5,15-bis[(4′-substituted-aryl)ethynyl]porphinato]-zinc(II) complexes (4′-substituents = F, MMe_2, H, OCH_3, CH_3, NO_2), which possess a_{2u}-derived HOMOs,[8] these ZINDO-based computational studies predict an a_{1u}-derived HOMO for **PZn( )NI** and **PZn[(F$_2$)NI]$_2$**. Consistent with the fact that the a_{1u} orbital possesses a node at the *meso*-carbon position, an examination of the dependence of the FO energies upon the relative donor, bridge, and acceptor torsional angles (Supporting Information) reveals that the extent of D−Sp−A conjugative interactions influence the relative energies of the HOMO-1 and lowest-lying porphyrin-localized unoccupied orbitals. Note, however, that the porphyrin-localized HOMO and LUMO levels for **PZn( )NI** differ by no more than ∼0.02 eV at maximal and minimal degrees of D−Sp−A π conjugation.

Electron Paramagnetic Resonance Spectroscopy. The nature of the PZn cation radical ($[PZn]^{\bullet+}$) species in these D−Sp−A systems was probed using electron paramagnetic resonance (EPR) spectroscopy. The cation radical states of both

(19) Imahori, H.; Tamaki, K.; Guldi, D. M.; Luo, C.; Fujitsuka, M.; Ito, O.; Sakata, Y.; Fukuzumi, S. *J. Am. Chem. Soc.* **2001**, *123*, 2607−2617.
(20) LeCours, S. M.; Guan, H.-W.; DiMagno, S. G.; Wang, C. H.; Therien, M. J. *J. Am. Chem. Soc.* **1996**, *118*, 1497−1503.
(21) Priyadarshy, S.; Therien, M. J.; Beratan, D. N. *J. Am. Chem. Soc.* **1996**, *118*, 1504−1510.
(22) LeCours, S. M.; Phillips, C. M.; dePaula, J. C.; Therien, M. J. *J. Am. Chem. Soc.* **1997**, *119*, 12578−12589.
(23) Karki, L.; Vance, F. W.; Hupp, J. T.; LeCours, S. M.; Therien, M. J. *J. Am. Chem. Soc.* **1998**, *120*, 2606−2611.
(24) Shediac, R.; Gray, M. H. B.; Uyeda, H. T.; Johnson, R. C.; Hupp, J. T.; Angiolillo, P. J.; Therien, M. J. *J. Am. Chem. Soc.* **2000**, *122*, 7017−7033.

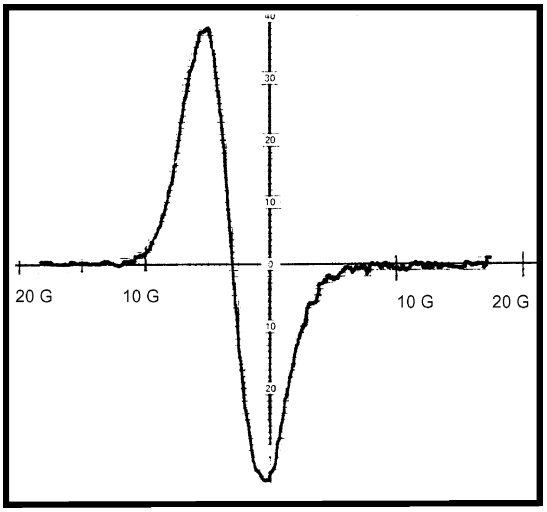

Figure 5. EPR spectrum of [**PZn( )PI**]$^{\bullet+}$ recorded in 19:1 methylene chloride:THF. Experimental conditions: temperature = 23 °C; modulation frequency = 100 Hz.

[**PZn( )PI**]$^{\bullet+}$ and [**PZn[( )NI]$_2$**]$^{\bullet+}$ were generated by the reaction of the neutral complexes with tris(4-bromophenyl)aminium hexachloroantimonate under oxygen-free conditions;[25] a representative EPR spectrum is shown in Figure 5. Note that no resolvable hyperfine splittings are evident in the EPR spectra of either [**PZn( )PI**]$^{\bullet+}$ or [**PZn[( )NI]$_2$**]$^{\bullet+}$, indicating that the HOMOs of these species possess a_{1u}-derived symmetry.

For [5,15-bis[(4′-substituted-aryl)ethynyl]porphinato]zinc(II) complexes, electronic interactions between the aryl and porphyryl units facilitated by the cylindrically π-symmetric ethyne moiety raise the energy of the a_{2u}-derived b_u/b_{1u} orbital above that of the a_{1u}-derived a_u orbital.[8] While strongly electron-withdrawing (4′-aryl)ethynyl substituents attenuate the magnitude of the b_u/b_{1u} orbital destabilization, an a_{2u}-like HOMO remains manifest even for [5,15-bis(4′-nitrophenyethynyl)-10,20-diphenylporphinato]zinc(II).[8] The D−Sp−A systems of Figure 1 feature *meso*-(aryl)ethynyl-derivatized PZn chromophores that possess electron-withdrawing 4′-NI/PI substituents, with experiment verifying the computational prediction of an a_{1u}-derived HOMO for these species. For [5,15-bis[(4′-substituted-aryl)-ethynyl]porphinato]zinc(II) complexes, the magnitude of the $b_u/b_{1u}-a_u$ energy gaps, as well as the absolute HOMO energy, track predictably with the Hammett σ_p value.[26] These data, coupled with an approximate Hammett σ_p value for PI and NI (0.33)[26] predict correctly the computed HOMO energy for these *meso*-[(4′-(NI/PI)-aryl)ethynyl]-derivatized PZn compounds with respect to the previously established benchmarks. While the $b_u/b_{1u}-a_u$ splittings for 5,15-bis[(4′-substituted-aryl)ethynyl]-porphinato]zinc(II) compounds decrease progressively from 0.27 to 0.1 eV with increasing values of the σ_p parameter [NMe_2 (−0.83), OMe (−0.27), H (0.0), F (0.06), NO_2 (0.78)],[8] a change in HOMO symmetry from b_u/b_{1u} to a_u for **PZn( )PI** and **PZn[( )NI]$_2$** is not predicted in such an analysis. One possible explanation for this spectroscopic perturbation evolves from Swain−Lupton dissection of the σ_p value into its inductive (F) and resonance (R) contributions.[27] While inductive and resonance effects contribute strongly to the magnitude of NO_2 group σ_p value, the σ_p parameter for cyclic imides is determined largely by the field (F) effect,[26] suggesting that the observed b_{1u} HOMO for [5,15-bis(4′-nitrophenyethynyl)-10,20-diphenylporphinato]-zinc(II) is not caused solely by a simple Hammett substituent effect but also from supplemental π-conjugative interactions between the porphyrin core and the nitrophenyl unit that destabilize the a_{2u}-derived orbital. Regardless of the precise origin of the a_u-symmetric HOMO observed for these D−Sp−A compounds (Figure 1), this electronic structural perturbation plays a key role in determining the nature of the ET dynamics delineated in these systems[28] as well as the relative magnitudes of the CS and CR rate constants (vide infra).

Analyses of the ET Dynamical Data. The ET rates determined from the pump−probe transient absorption spectroscopic studies were analyzed using the semiclassical Marcus−Levich−Jortner eq 1.[29−32]

$$k_{ET} = \frac{2\pi}{\hbar}\frac{H_{AB}{}^2}{\sqrt{4\pi\lambda_S k_B T}}\exp(-S_c)\sum_{m=0}^{\infty}\frac{S_c{}^m}{m!}\times \exp\left(-\frac{(\Delta G + \lambda_s + m\hbar\langle\omega\rangle)^2}{4\lambda_s k_B T}\right) \quad (1)$$

In eq 1, $\hbar$ is Planck's constant, H_{AB} is the electronic coupling, k_B is Boltzman's constant, λ_s is the solvent reorganization energy, S_c is the Huang−Rhys factor ($S_c = \lambda_i/[\hbar\langle\omega\rangle]$), where λ_i is the inner sphere reorganization energy, $\langle\omega\rangle$ is the averaged frequency of the high-frequency vibrations in the reactant state, and m is the number of vibrational levels**.** The ΔG values were determined using the standard Weller eqs 2 and 3;[33] (Table 2). The solvent reorganization energy (λ_S) was calculated by the Marcus relation (eq 4).[29]

$$\Delta G_{CS} = e(E_{ox} - E_{red}) - E_{0,0} - \frac{e^2}{4\pi\epsilon_o\epsilon_s R_{DA}} + \frac{e^2}{4\pi\epsilon_o}\left(\frac{1}{\epsilon_s} - \frac{1}{\epsilon_s^{ref}}\right)\left(\frac{1}{\epsilon_s} - \frac{1}{\epsilon_s^{ref}}\right)\left(\frac{1}{2R_D} + \frac{1}{2R_A}\right) \quad (2)$$

$$\Delta G_{CR} = -\Delta G_{CS} - E_{0,0} \quad (3)$$

$$\lambda_s = \frac{e^2}{4\pi\epsilon_0}\left(\frac{1}{n^2} - \frac{1}{\epsilon_s}\right)\left(\frac{1}{2R_D} + \frac{1}{2R_A} - \frac{1}{R_{DA}}\right) \quad (4)$$

The D (R_D) and A (R_A) reactant sizes, and the center-to-center distance (R_{DA}) between D and A were determined from D−Sp−A conformations optimized by the MOPAC-AM1 method. H_{AB} and λ_i were the only adjustable parameters used in the global fit of the dynamical data; in this computational analysis, λ_i was assigned a value of 0.3 eV,[34] a reasonable value for these D−Sp−A systems, given literature precedent,[9,35] and was allowed to range within ±0.1 eV of this initial estimate.

(25) Shultz, D. A.; Lee, H.; Gwaltney, K. P. *J. Org. Chem.* **1998**, *63*, 7584−7585.
(26) Hansch, C.; Leo, A.; Taft, R. W. *Chem. Rev.* **1991**, *91*, 165−195.
(27) Swain, C. G.; Lupton, E. C., Jr. *J. Am. Chem. Soc.* **1968**, *90*, 4328−4337.
(28) Strachan, J.-P.; Gentemann, S.; Seth, J.; Kalsbeck, W. A.; Lindsey, J. S.; Holten, D.; Bocian, D. F. *J. Am. Chem. Soc.* **1997**, *119*, 11191−11201.
(29) Marcus, R. A. *J. Chem. Phys.* **1965**, *43*, 679−701.
(30) Levich, V. G. *Adv. Electrochem. Electrochem. Eng.* **1966**, *4*, 249−371.
(31) Ulstrup, J.; Bixon, M. *J. Chem. Phys.* **1975**, *63*, 4358−4368.
(32) Efrima, S.; Bixon, M. *Chem. Phys.* **1976**, *13*, 447−460.
(33) Weller, A. Z. *Phys. Chem. N. F.* **1983**, *133*, 93−98.
(34) Rubtsov, I. V.; Shirota, H.; Yoshihara, K. *J. Phys. Chem. A* **1999**, *103*, 1801−1808.
(35) Osuka, A.; Noya, G.; Taniguchi, S.; Okada, T.; Nishimura, Y.; Yamazaki, I.; Mataga, N. *Chem.−Eur. J.* **2000**, *6*, 33−46.

Table 3. Comparison of Experimentally Determined Photoinduced CS Rates with Those Predicted by the Marcus−Levitch−Jortner Equation

					benzene		methylene chloride		acetonitrile	
compound	R_D (Å)	R_A (Å)	R_{DA} (Å)	H_{AB} (cm^{-1})	k_{CS}(exp) (ps^{-1})	k_{CS}(calc) (ps^{-1})	k_{CS}(exp) (ps^{-1})	k_{CS}(calc) (ps^{-1})	k_{CS}(exp) (ps^{-1})	k_{CS}(calc) (ps^{-1})
PZn( )PI[a]	4.0	3.6	15	50	0.0093	3.1×10^{-6}	0.041	0.018	0.0067	0.008
PZn[( )NI]$_2$[a]	4.0	3.8	15.2	50	0.083	0.018	0.043	0.076	0.030	0.034
PZn[(CH_3)NI]$_2$[b]	4.0	3.8	15.2	50	0.065	0.039	0.100	0.067	0.022	0.031

[a] $\lambda_i = 0.3$ eV. [b] $\lambda_i = 0.35$ eV.

Table 4. Comparison of Experimentally Determined Thermal CR Rates with Those Predicted by the Marcus−Levitch−Jortner Equation

					benzene		methylene chloride		acetonitrile	
compound	R_D (Å)	R_A (Å)	R_{DA} (Å)	H_{AB} (cm^{-1})	k_{CR}(exp) (ps^{-1})	k_{CR}(calc) (ps^{-1})	k_{CR}(exp) (ps^{-1})	k_{CR}(calc) (ps^{-1})	k_{CR}(exp) (ps^{-1})	k_{CR}(calc) (ps^{-1})
PZn( )PI[a]	3.6	4.0	15	75	0.005	3.5×10^{-6}	0.95	0.97	0.37	0.15
PZn[( )NI]$_2$[a]	3.8	4.0	15.2	50	0.0023	7.2×10^{-6}	0.16	0.41	0.45	0.034
PZn[(CH_3)NI]$_2$[b]	3.8	4.0	15.2	50	0.014	1.8×10^{-5}	0.10	0.39	0.21	0.027

[a] $\lambda_i = 0.3$ eV. [b] $\lambda_i = 0.35$ eV.

Table 5. Comparison of Experimentally Determined Photoinduced CS Rates with Those Predicted by the Marcus−Levitch−Jortner Equation Using Expanded R_D and R_A

				benzene		methylene chloride		acetonitrile	
compound	R_D (Å)	R_A (Å)	H_{AB} (cm^{-1})	k_{CS}(exp (ps^{-1})	k_{CS}(calc) (ps^{-1})	k_{CS}(exp) (ps^{-1})	k_{CS}(calc) (ps^{-1})	k_{CS}(exp) (ps^{-1})	k_{CS}(calc) (ps^{-1})
PZn( )PI[a,b]	7.7	3.6	10	0.0093	0.017	0.041	0.020	0.0067	0.020
PZn[( )NI]$_2$[a]	7.7	3.8	15	0.083	0.030	0.043	0.035	0.030	0.039
PZn[(CH_3)]NI$_2$[c]	7.7	3.8	15	0.065	0.022	0.10	0.032	0.022	0.037

[a] $\lambda_i = 0.3$ eV. [b] $R_{DA} = 7.7$ Å. [c] $\lambda_i = 0.35$ eV.

Table 6. Comparison of Experimentally Determined Thermal CR Rates with Those Predicted by the Marcus−Levitch−Jortner Equation Using Expanded R_D and R_A

				benzene		methylene chloride		acetonitrile	
compound	R_D (Å)	R_A (Å)	H_{AB} (cm^{-1})	k_{CR}(exp) (ps^{-1})	k_{CR}(calc) (ps^{-1})	k_{CR}(exp) (ps^{-1})	k_{CR}(calc) (ps^{-1})	k_{CR}(exp) (ps^{-1})	k_{CR}(calc) (ps^{-1})
PZn( )PI	3.6	7.7	100	0.005	0.002	0.95	0.16	0.37	0.35
PZn[( )NI]$_2$	3.8	7.7	55	0.0023	0.003	0.16	0.20	0.45	0.42
PZn[(CH_3)NI]$_2$	3.8	7.7	40	0.014	0.007	0.10	0.17	0.21	0.26

The ET rate constants calculated in this manner, obtained using D, A, and R_{DA} sizes from geometry optimized structures, agree well with the k_{CS} values determined via pump−probe transient optical spectroscopic measurements (Table 3). The experimentally determined CR rate constants, however, differ dramatically from the values predicted by the classic Marcus−Levich−Jortner analysis (Table 4). Among the possible explanations for this disparity is that the (aryl)ethynyl bridging unit facilitates augmented delocalization of the CS state with respect to the ground and singlet-excited states, rather than playing a passive role in the ET dynamics of these conjugated D−Sp−A arrays. The notion that a highly π-conjugated bridging unit can augment the magnitude of donor or acceptor electronic delocalization to form a "superdonor" or "superacceptor"[15] has been discussed previously. Singer has shown in a series of *p*-polyphenylamines that aromatic bridging units can act as an extension of the D or A moieties in charge-transfer reactions,[3] and Khundkar has reported the involvement of a π-conjugated bridge in the excited state CR reactions of asymmetrically substituted di-(aryl)ethynyl molecules.[4] More recently, Brédas has implicated the formation of superdonors/superacceptors in the ET dynamics of a series of compounds in which *p*-phenylene vinylene bridges link a tetracene donor to a pyromellitic diimide acceptor.[5,7]

Accordingly, the ET rate constants were recalculated, treating the D and A reactant sizes in the excited and CS states as adjustable parameters. While such a procedure has little impact on the quality of the fit obtained for the CS ET rate data, considerably better fits of the CR dynamical data were generated; this improvement in fit quality was most dramatic for the symmetric D−Sp−A systems **PZn[( )NI]$_2$** and **PZn[(CH_3)NI]$_2$** (Tables 5 and 6). The reactant size of either (or both) the [$(PZn)^{\bullet+}$] acceptor or the $PI^{\bullet-}$/$NI^{\bullet-}$ donor were increased to include the (aryl)ethynyl bridging unit; the extent to which these theoretical and experimental results correlate can be depicted graphically. Figure 6 compares CR rate constants computed via the Marcus−Levich−Jortner equation using both restricted and expanded radical ion reactant sizes to those measured experimentally for **PZn[( )NI]$_2$**. The CR rate constants, calculated with one enlarged radical ion size, fit the experimental data well (Figure 6); when the radical ion reactant sizes were restricted to the $PZn^{\bullet+}$ and $NI^{\bullet-}$ units, the quality of the fit dropped dramatically (Figure 6). The CS rate constants calculated for

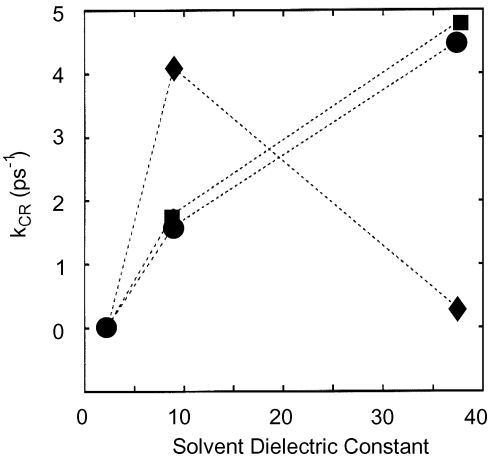

Figure 6. Graphical comparison of experimentally determined **PZn[( )-NI]$_2$ CR** rate constants (●) with those computed theoretically via the Marcus−Levich−Jortner equation using D- and A-localized radical ion sizes (♦) and with a $PZn^{\bullet+}$ acceptor that is delocalized over the (aryl)ethynyl spacer (■).

PZn[( )NI]$_2$ using either small (Table 3) or large (Table 5) ion sizes correlate well with the experimental CS rates (data not shown); note that expansion of D and A reactant sizes to include the bridge in the analysis of the CS reaction dynamics requires a concomitant drop in electronic coupling.

While expanded reactant sizes are clearly implicated in the CR reactions of these D−Sp−A assemblies, key questions that need to be addressed include: (1) To what extent are the electronically excited states of these ET arrays delocalized? and (2) Is it the PZn cation radical or the diimide anion radical (or both) that is delocalized over the bridge in the charge-separated state? Some insight into this issue can be obtained by examining how reducing π-overlap of either D or A with the conjugated bridge affects the observed ET dynamics, as attenuated conjugation should diminish excited- and CS-state delocalization.

Comparative ET Dynamics in PZn[(CH$_3$)NI]$_2$ and PZn-[( )NI]$_2$: Determining the Degree of Sp-A Delocalization. We first examine the degree of delocalization between the (aryl)-ethynyl bridge and the diimide acceptor in the excited and CS states. Introducing additional steric hindrance between the Sp-phenyl ring ortho substituents and the A diimide amide oxygens increases the energy of Sp-A conformeric populations having small phenyl-PI/NI interplanar torsional angles and thereby reduces the extent of π-conjugation between Sp and A in the ground, excited, and charge-separated states. Molecular modeling studies (Experimental Section, Supporting Information) suggest that the ortho-methyl substituent in **PZn[(CH$_3$)NI]$_2$** is sufficient to ensure a significant reduction in the range of thermally accessible torsional angles, θ, between the NI acceptor and the Sp-phenyl ring; notably, this bridge ortho-methyl substitution has negligible impact on the ET thermodynamics (Table 2).

If bridge ortho-methylation modulates the ET dynamics in **PZn[(CH$_3$)NI]$_2$** relative to **PZn[( )NI]$_2$** to an extent greater than that predicted by theory on purely thermodynamic grounds, such data would lend support to the hypothesis that augmented Sp-A electronic delocalization plays a role in the ET reactions of the systems. With respect to the CS reactions for these species, if Sp-A electronic delocalization were important, the impact of attenuated conjugation in **PZn[(CH$_3$)NI]$_2$** relative to **PZn[( )-NI]$_2$** should be evident in the fit of the ET dynamics. The Marcus−Levich−Jortner equation, however, predicts only a small change in the magnitude of k_{CS} in these systems, which is consistent with the experimental observation (Table 3), and indicates that Sp-A electronic delocalization is not a determinant of the magnitude of k_{CS} in these systems.

An analogous examination can be made of the **PZn[(CH$_3$)-NI]$_2$** CR reaction. An identical theoretical analysis predicts that bridge methylation should have modest impact on the **PZn-[(CH$_3$)NI]$_2$** CR dynamics with respect to that observed for **PZn[( )NI]$_2$** in nonpolar solvents such as benzene. Again, theory and experiment correlate (Table 4). While the absolute magnitude of k_{CR} for these compounds is not modeled well by these Marcus−Levich−Jortner calculations, note that theory does predict the trend in the relative magnitudes of k_{CR} for these species; this rules out the possibility that enhanced Sp-A electronic delocalization within the CS state plays a role in the CR dynamics. However, because augmented reactant size is crucial for a reasonable fit of the CR rate data, these data imply that it is the PZn cation radical that delocalizes onto the (aryl)-ethynyl unit in the CS state.

Solvent Dependence of CR in PZn[(CH$_3$)NI]$_2$. On the basis of the Marcus−Levich−Jortner analysis of the CS reaction rate data, the initially prepared CS state is not highly delocalized (vide supra); the key remaining issue involves whether the CS state undergoes a change, either in geometry or in polarization, before the CR reaction occurs. Analysis of the CR rate data obtained for **PZn[(CH$_3$)NI]$_2$** and **PZn[( )NI]$_2$** argue that if any augmented delocalization of the CS state occurs, it does not involve an appreciable change in the nature of Sp-A electronic interactions. To further support the hypothesis that the initially formed $PZn^{\bullet+}$ delocalizes onto the (4′-phenyl)ethynyl bridge, we examine the CR dynamics for **PZn[(CH$_3$)NI]$_2$** in viscous solvent; an increase in the time constant for diffusional rotation of the Sp phenyl ring is expected with increased solvent viscosity.[36−41] The ET dynamics exhibited by **PZn[(CH$_3$)NI]$_2$** in polystyrene were compared to those established in benzene, as these two solvents feature similar dielectric constants but highly disparate viscosities.

τ_{CR} for **PZn[(CH$_3$)NI]$_2$** in polystyrene is 900 ps, more than 10-fold larger than the analogous time constant determined in benzene (Table 1). This substantial difference in the magnitudes of k_{CR} in polystyrene and benzene supports the propositions that: (i) the angle formed between the phenyl and porphyrin rings is an important determinant of CR dynamics, and (ii) the time scale for $PZn^{\bullet+}$-Sp electronic delocalization is likely a function of aryl ring rotational time constant in these (phenyl)-ethynyl bridged D−A arrays.

Pump-Wavelength Dependence of the Magnitude of k_{CS} in PZn[( )NI]$_2$ and PZn[(CH$_3$)NI]$_2$. The proposition that the extent of CS state electronic delocalization depends at least in part upon aryl ring rotational dynamics, suggests, together with the Marcus−Levich−Jortner-based ET dynamical analyses, that

(36) LaChapelle, M.; Belletête, M.; Poulin, M.; Godbout, N.; LeGrand, F.; Héroux, A.; Brisse, F.; Durocher, G. *J. Phys. Chem.* **1991**, *95*, 9764−9772.
(37) Abedin, K. M.; Ye, J. Y.; Inouye, H.; Hattori, T.; Hitoshi, S.; Nakatsuka, H. *J. Chem. Phys.* **1995**, *103*, 6414−6425.
(38) Chen, Y.; Wu, S.-K. *J. Photochem., Photobiol., A* **1997**, *102*, 203−206.
(39) Yee, W. A.; O'Neil, R. H.; Lewis, J. W.; Zhang, J. Z.; Kliger, D. S. *J. Phys. Chem. A* **1999**, *103*, 2388−2393.
(40) van der Meer, M. J.; Zhang, H.; Glasbeek, M. *J. Chem. Phys.* **2000**, *112*, 2878−2887.
(41) Tan, X.; Gustafson, T. L. *J. Phys. Chem. A* **2000**, *104*, 4469−4474.

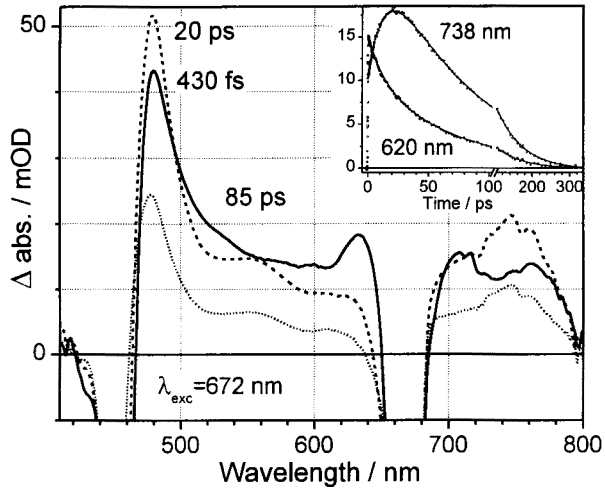

Figure 7. Transient absorption spectra of **PZn[(CH$_3$)NI]$_2$** in benzene, with labeled time delays. Inset shows transient kinetics measured at 738 and 620 nm, which probe the formation of the CS state. Experimental conditions: $\lambda_{ex} = 672$ nm, temperature $= 23 \pm 1$ °C.

Table 7. Charge Separation and Charge Recombination Dynamical Data Determined from Pump−Probe Transient Absorption Spectroscopic Measurements at Varying Excitation Wavelengths (λ_{ex}) in Benzene Solvent

compound	λ_{ex} (nm)	τ_{CS} (ps)	k_{CS} (s^{-1})	τ_{CR} (ps)	k_{CR} (s^{-1})	τ_{CR}/τ_{CS}
PZn[( )NI]$_2$	645	16	6.3×10^{10}	500	2×10^{9}	32
	672	12	8.3×10^{10}	430	2.3×10^{9}	36
PZn[(CH$_3$)]NI$_2$	645	18	5.6×10^{10}	71	1.4×10^{10}	4.0
	655	16	6.3×10^{10}	74	1.4×10^{10}	4.8
	672	13	7.7×10^{10}	71	1.4×10^{10}	5.4

the initially prepared excited-states of these complexes are largely PZn-localized. Whether or not the Franck−Condon state initially formed upon excitation undergoes geometrical changes leading to the formation of a lower-energy, more coplanar state that facilitates augmented D-Sp delocalization can be determined from an examination of the pump-wavelength dependence of the CS dynamics.

The lowest-lying singlet-excited state of *meso*-(aryl)ethynyl-substituted porphyrins has been determined to be polarized along the *x*-axis; the spectral heterogeneity of the Q_x-transition envelope of these species derives from conformeric populations that differ in the extent of conjugation between the (aryl)ethynyl arene and the porphyrin core.[8] Exciting a population of ground-state molecules in which the geometry resembles the low-energy excited state (red-edge excitation of the $Q_x(0,0)$ envelope) should effect an increase in CS rate constant; likewise pump wavelengths that correspond to the blue-edge of the $Q_x(0,0)$ manifold selectively excite a population of less conjugated conformers. Figure 7 displays the relevant transient absorption spectra for **PZn[(CH$_3$)NI]$_2$**, while Table 7 tabulates the excitation-wavelength-dependent dynamical data obtained for **PZn[( )NI]$_2$** and **PZn[(CH$_3$)NI]$_2$**.

The pump wavelength dependences of the CS dynamics for **PZn[( )NI]$_2$** and **PZn[(CH$_3$)NI]$_2$** show that the average τ_{CS} measured in benzene decreases only slightly with longer excitation wavelength (λ_{ex}), varying from 17.9 to 13.2 ps for **PZn[(CH$_3$)NI]$_2$** and from 15.7 to 10.8 ps for **PZn[( )NI]$_2$** for λ_{ex} ranging from 645 to 672 nm (Table 7), suggesting that the extent of electronic delocalization in the initially prepared S_1 state varies only modestly with the excitation wavelength. It is interesting that these data are incongruent with the established photophysics of [5,15-bis[(aryl)ethynyl]-10,20-diphenylporphinato]zinc(II) compounds.[8,20−23] This result likely derives in part from differences in the configuration expansion that describes the S_1-excited state for **PZn[( )NI]$_2$** and **PZn[(CH$_3$)NI]$_2$** with respect to previously studied [5,15-bis[(aryl)ethynyl]-10,20-diphenylporphinato]zinc(II) compounds;[8,20,22] in contrast to these benchmarks, [5,15-bis[4′-(*N*-(*N*′-octyl)pyromellitic/naphthylic diimide)aryl)ethynyl]-10,20-diphenylporphinato]zinc-(II) complexes possess a_{1u}-derived HOMOs. Importantly, however, the relatively minor dependence that CS rate constants have upon λ_{ex} is consistent with the expectation derived from the theoretical analysis of the ET dynamical data (vide supra) that suggests that the excited states of these D−Sp−A assemblies are largely PZn-localized and that (aryl)ethynyl bridge participation in electronic delocalization augmentation is confined to the CS state.

Conclusions

The solvent-dependent ET dynamics of a series of [5-[4′-(*N*-(*N*′-octyl)pyromellitic/naphthylic diimide)aryl)ethynyl]-10,20-diphenylporphinato]zinc(II) and [5,15-bis[4′-(*N*-(*N*′-octyl)-pyromellitic/naphthylic diimide)aryl)ethynyl]-10,20-diphenylporphinato]zinc(II) complexes have been determined via time-resolved transient absorption spectroscopy. Marcus−Levich−Jortner analysis of these data shows that, in contrast to the charge-separation reaction dynamics, the magnitudes of the experimentally determined CR rate constants cannot be fit using this model if the CS states of these D−Sp−A systems feature conventional D- and A-localized reactant sizes. This analysis, coupled with electronic structure calculations, potentiometric experiments, and additional pump-wavelength- and solvent-viscosity dynamical data, indicates that the initially formed CS states of these species relax to more delocalized CS states in which the porphyrin macrocycle and (4′-phenyl)ethyne bridge form a π-conjugated "super acceptor";[3,4,7,42] thus, while the (aryl)ethynyl Sp simply mediates electronic superexchange for photoinduced charge separation, it plays a nonpassive role in thermal CR processes.

The expansion of A cation size within the CS state (i) causes the effective D−A edge-to-edge distance in these (aryl)ethynyl-bridged PZn−PI/NI compounds to differ little from that defined by directly linked **PZnPI** (Figure 1) and (ii) attenuates severely the dependence of the magnitudes of the CR rate constants upon solvent. The established CR dynamics, coupled with the solvent dependence of the Marcus−Levich−Jortner-computed ($\Delta G°_{CR} + \lambda_T$) values, underscore this latter point: as solvent polarity is varied from acetonitrile to benzene, analyses which utilize D- and A-localized reactant states show that the quantity ($\Delta G°_{CR} + \lambda_T$) takes on values that range from 0.7 to −1.9 eV. In contrast, when the effect of a conjugation-expanded PZn cation radical is considered, ($\Delta G°_{CR} + \lambda_T$) spans −0.25 to −1.28 eV between these extremes of solvent polarity.

In these D−Sp−A assemblies, the σ-electron-withdrawing 4′-(aryl)ethynyl substituents influence ground-state electronic structure; both EPR spectroscopy and theory show that these D−Sp−A assemblies possess a_{1u}-derived HOMOs. Electronic delocalization in the CS state, however, is unlikely to be

(42) Davis, W. B.; Svec, W. A.; Ratner, M. A.; Wasielewski, M. R. *Nature* **1998**, *396*, 60−63.

facilitated by an a_{1u}-derived HOMO, as it possesses a node at the *meso*-position. Given the close D−A distances in these D−Sp−A systems, the nature of the Sp electronic structure, and the fact that the classic Gouterman a_{1u}- and a_{2u}-derived FOs are predicted to lie very close in energy (Figure 4 and Supporting Information), Coulombic interactions between D^+ and A^- likely drive an a_{1u}-a_{2u} orbital inversion in the CS state. The analysis of the CR rate data obtained in viscous media suggests that an electronic structural rearrangement is likely coupled tightly to diffusive rotation of the Sp unit aryl ring. Consistent with such an analysis, the CS and CR reactions for **PZn( )( )PI**, which has a larger D−A distance and therefore reduced D^+/A^- Coulombic interaction, does not display the reverse kinetics ($k_{CR} \gg k_{CS}$) associated with the remainder of this series of compounds (Table 1).

Finally, while these data indicate that simple (aryl)ethynyl units can facilitate augmented CS-state hole delocalization over the D−A length scales probed in this study, it is important to emphasize that this work, coupled with earlier investigations,[8,21−23] highlights as well that the extent of singlet-excited-state wave function amplitude on the arylethynyl moiety is a sensitive function of arene electronic structure; hence, engineering the extent to which the (aryl)ethyne bridge delocalizes D- or A-centered electron density, in both photoinduced CS and thermal CR reactions within this class of compounds, should be amenable to modulation via molecular design.

Acknowledgment. We thank Professor Paul J. Angiolillo (St. Joseph's University) and Dr. Thomas Troxler (NIH Regional Laser Laboratory, University of Pennsylvania) for their respective assistance with EPR and time-correlated single-photon counting spectroscopic measurements. This work was supported by a grant from the Division of Chemical Sciences, Office of Basic Energy Research, U.S. Department of Energy (DE-FGO2-02ER15299). M.J.T. thanks the Office of Naval Research (N00014-97-0317) and the MRSEC Program of the National Science Foundation (DMR-00-79909) for equipment grants for transient optical instrumentation.

Supporting Information Available: Complete details of the synthesis and characterization of the series of compounds, and synthetic schemes. Transient- and steady-state optical spectra of **PZn(F_2)NI**, **PZn( )PI**, **PZn[( )PI]$_2$**, and **PZn[( )NI]$_2$** in methylene chloride, transient optical spectra of **PZn( )PI** and **PZn[(CH_3)NI]$_2$** in acetonitrile, and tabulated cyclic voltammetric data. Both tabulated and graphic HOMO-1, HOMO, LUMO, and LUMO+1 energies for **PZn( )NI**. and MOPAC-calculated phenyl ring rotational barriers for **PZn[( )NI]$_2$** and **PZn[(CH_3)-NI]$_2$** (PDF). This material is available free of charge via the Internet at http://pubs.acs.org.

JA021278P